

Supplement of Atmos. Meas. Tech., 12, 5231–5246, 2019
<https://doi.org/10.5194/amt-12-5231-2019-supplement>
© Author(s) 2019. This work is distributed under
the Creative Commons Attribution 4.0 License.



Supplement of

Characterisation of the transfer of cluster ions through an atmospheric pressure interface time-of-flight mass spectrometer with hexapole ion guides

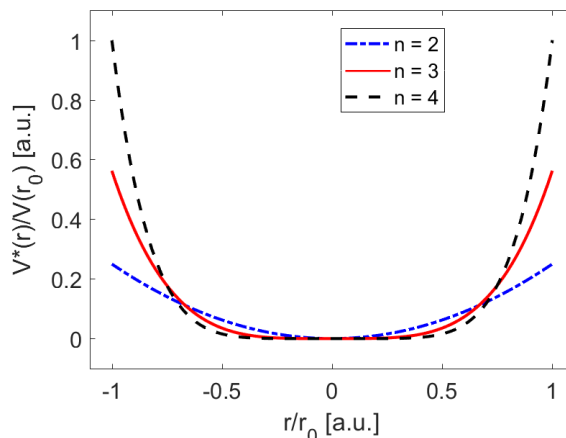
Markus Leiminger et al.

Correspondence to: Gerhard Steiner (gerhard.steiner@uibk.ac.at) and Armin Hansel (armin.hansel@uibk.ac.at)

The copyright of individual parts of the supplement might differ from the CC BY 4.0 License.

1

2 The discussion about the effective potential is visualised with Fig. S0. Here, the effective potential is normalised to $V(r_0)$ and
 3 scaled to the maximum of the octopole. This shows that higher multipoles have an increased effective potential close to the
 4 rods where r/r_0 approaches 1 and are flatter close to the centre axis.



5

6

Figure S0: Effective potential for three types of multipoles; quadrupole ($n=2$), hexapole ($n=3$) and octopole ($n=4$).

7

8 Supplementary material about the transmission efficiency

9 Here, we provide additional information about the way we determined the transmission efficiency of both mass spectrometers.
 10 Electrospray ionisation (ESI) of tetra-alkyl-ammonium halides leads to the formation of tetra-alkyl-ammonium ions. A voltage
 11 scan with the Differential Mobility Analyser (UDMA) used in this study generates an ion mobility spectrum exemplarily
 12 shown in Fig. S1a for Tetra-Butyl-Ammonium Iodide. The corresponding mass spectrum averaged over the full ion mobility
 13 spectrum is given in Fig. S1b. Applying a constant voltage to the UDMA that corresponds to a specific electrical mobility of
 14 an ion, generates a constant stream of only ions of the selected electrical mobility. In Fig. S2, we show examples of mass
 15 spectra for classified monomer, dimer and trimer ions of Tetra-Butyl-Ammonium Iodide. In the mass spectrum of the TBAI
 16 trimer, fragment peaks at the m/z of the monomer and the dimer are visible. Similarly, a monomer fragment peak appears in
 17 the mass spectrum of the dimer. As described in the main text, the transmission efficiency for dimers and trimers was corrected
 18 in an iterative process for fragment peaks. First, the transmission efficiency of the monomer was determined. The electrometer
 19 signal of the classified dimer was corrected for the fraction of monomer fragment signals in the dimer mass spectrum using
 20 the monomer's transmission efficiency. Accordingly, we corrected the electrometer signal of the classified trimer using the
 21 dimer's and monomer's transmission efficiency. The following relationships were used for the calculations, with e_0 as the
 22 elementary charge, I_{FCE} the ion-induced current in fA, Q_{FCE} the flow rate through the FCE in L/min, $Q_{TOF, \text{pinhole}}$ the flow into
 23 the TOF mass spectrometer, signal_{TOF} the signal of all isotopes of a calibration compound in counts per second and $[\text{ion}]_{FCE}$
 24 the ion number concentration calculated from the current in ions per cm^3 .

25

26

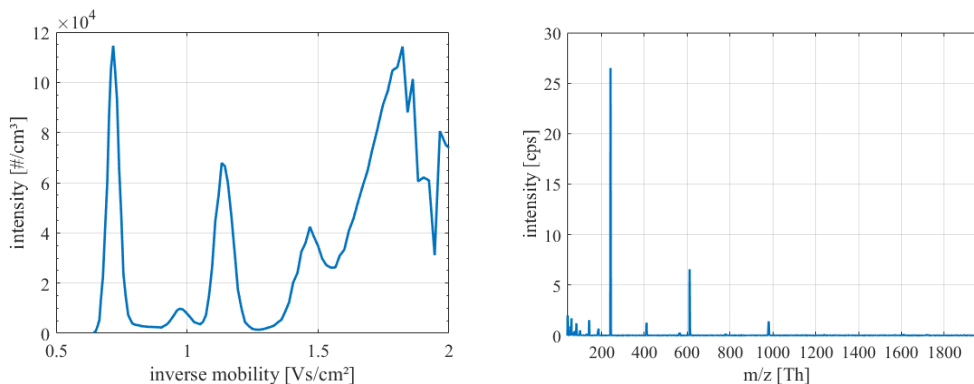
$$[\text{ions}]_{FCE} = \frac{I_{FCE}}{e_0 \cdot Q_{FCE}} \quad (\text{E1})$$

27

28

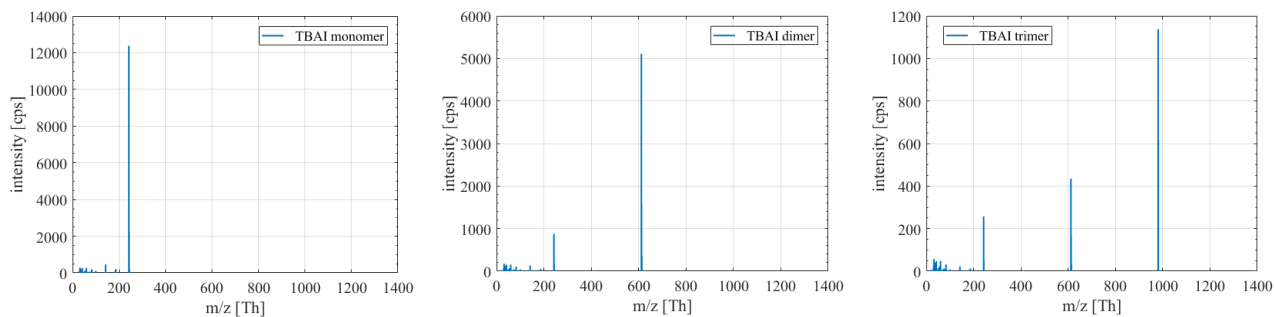
$$transmission = \frac{signal_{TOF}}{[ions]_{FCE}} \cdot \frac{1}{Q_{TOF,pinhole}} \quad (E2)$$

29



30

31 **Figure S1:** left) ion mobility spectrum acquired with the Faraday Cup Electrometer, right) mass spectrum with the ioniAPi-TOF averaged
32 over the full scan of the ion mobility spectrum.



33

34 **Figure S2:** Mass spectra showing the classified monomer, dimer and trimer ions of Tetra-Butyl-Ammonium Iodide.

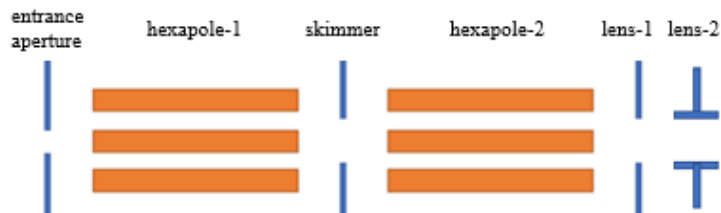
35

36 Supplementary material about the ion transfer characterisation

37

38 To support the data shown in Fig. 7, we examined further experiments. Additional declustering scans were done between
39 different ion optic components in the ioniAPi-TOF. These experiments were conducted with a high-resolution ioniAPi-TOF.
40 The mass resolving power of this instrument is about 6000. The components, electronics, geometries and conditions inside the
41 instrument are almost identical to the one described in the main text. The only difference aside from the mass resolving power
42 and the length of the mass analyser is the length of hexapole-2. The hexapole-2 from the main text has a length of 3 cm, while
43 the one installed in the high resolution ioniAPi-TOF has a length of 5 cm. This has only minor impact on the following results
44 as can be seen in the following. The slightly longer hexapole-2 will mainly lead to a small increase of the residence time of

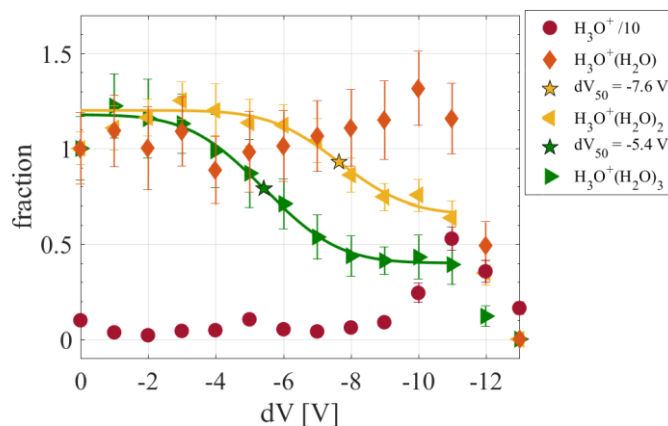
45 the ions within the ion guide but should not affect much the voltage scans from the hexapole to the neighbouring ion optic
 46 components.



47

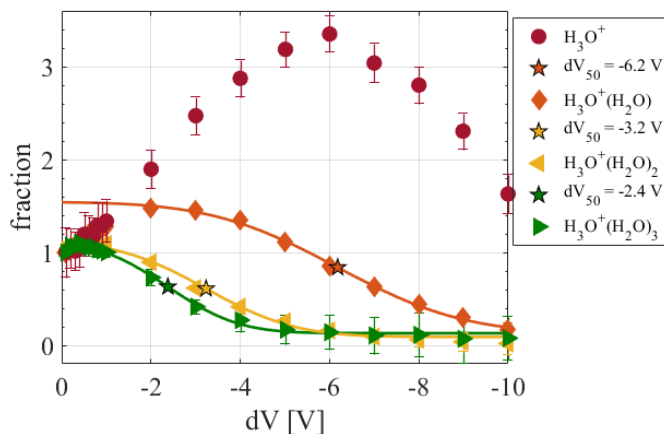
48

Figure S3: Extended schematic of the ion optics of the ioniAPi-TOF mass spectrometer.



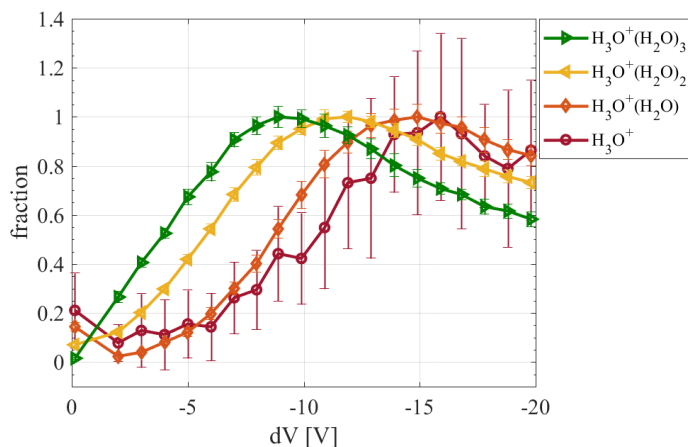
49

50 **Figure S4:** Decustering (dV) scan with the high resolution ioniAPi-TOF 6000 in analogy to Fig. 7 from the main text. Here, nearly
 51 identical electric potentials were used compared to the previous ioniAPi-TOF. The electric potential at lens-1 that follows hexapole-2 is set
 52 to -13 V. All electric potentials upstream of hexapole-2 are set to 0 V. The ion optics downstream of lens-2 are constant for all data shown
 53 in the supplementary. Similar dV_{50} values could be obtained indicating that the following results should in principle also be applicable to
 54 the ioniAPi-TOF from the main text. Below -12 V, all cluster ions decrease due to a lower transmission efficiency. The signal of H_3O^+ is
 55 divided by 10 for clarity.



56

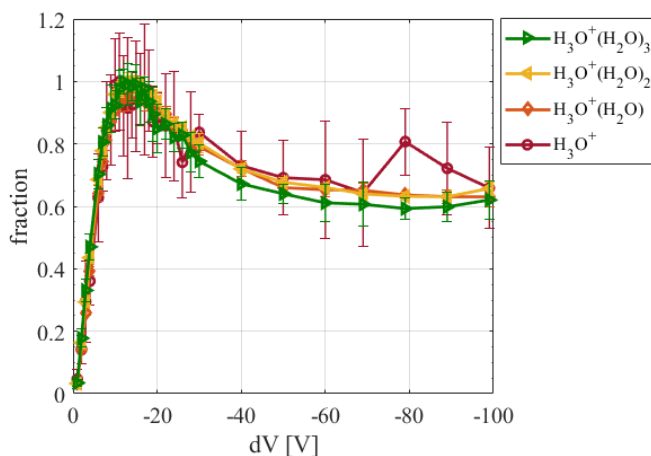
57 **Figure S5:** Declustering scan between the skimmer and the second hexapole. The potential difference between hexapole-2 and lens-1 is
 58 always 1 V as they are stepwise increased to maintain transmission. Determined dV_{50} values are -2.3, -3.2 and -6.2 V for the hydronium
 59 cluster ions $\text{H}_3\text{O}^+(\text{H}_2\text{O})_3$, $\text{H}_3\text{O}^+(\text{H}_2\text{O})_2$ and $\text{H}_3\text{O}^+(\text{H}_2\text{O})_1$. The obtained dV_{50} values are lower compared to Fig. S2. This indicates that the
 60 higher electric potential of -13 V at lens-1 most likely has introduced an offset to the expected fragmentation between skimmer and
 61 hexapole-2. Here, already lower voltages can lead to dissociation of the hydronium clusters. At least -2.3 V are necessary to dissociate 50
 62 % of $\text{H}_3\text{O}^+(\text{H}_2\text{O})_3$ that has a binding energy of 17 kcal/mol. For lower voltages, fragmentation of cluster ions with similar binding energies
 63 will be less significant. Regarding the ion transmission efficiency, no or only small DC offset voltages need to be applied to hexapole-2 for
 64 suitable ion transmission. So, the ion transfer optics can be set to low fragmenting settings and still enabling an adequate ion transmission.



65

66 **Figure S6:** Declustering scan between the second hexapole and lens-1. Signals are scaled to the maximum signal for clarity. All electric
 67 potentials upstream lens-1 are at 0 V. The potential difference between lens-1 and lens-2 is 0 V as they are evenly increased.
 68 Fragmentation of $\text{H}_3\text{O}^+(\text{H}_2\text{O})_3$ only starts above a dV of -9 V. This scan shows that this region needs to be set to a rather high electric
 69 potential to enable significant fragmentation of cluster ions. While this region can also be used for fragmentation experiments, it also
 70 offers a broad range of settings for low fragmenting transfer.

71



72

73 **Figure S7:** Voltage scan between the second lens-1 and lens-2. Signals are scaled to the maximum signal for clarity. All electric potentials
 74 upstream lens-2 are at 0V. This voltage scan has an almost exclusive impact on the transmission efficiency independent of the mass-to-
 75 charge ratio and no obvious impact on the stability of cluster ions.